

SPIDERS IN LYOT CORONAGRAPHS

ANAND SIVARAMAKRISHNAN,¹
Space Telescope Science Institute
3700 San Martin Drive, Baltimore, MD 21218

AND

JAMES P. LLOYD¹
Department of Astronomy
230 Space Sciences Building
Cornell University
Ithaca, NY 14853
Accepted ApJ June 2005

ABSTRACT

In principle, suppression of on-axis stellar light by a coronagraph is easier on an unobscured aperture telescope than on one with an obscured aperture. Recent designs such as the apodized pupil Lyot coronagraph, the ‘band-limited’ Lyot coronagraph, and several variants of phase mask coronagraphs work best on unobscured circular aperture telescopes. These designs are developed to enable the discovery and characterization of nearby jovian or even terrestrial exoplanets. All of today’s major space-based and adaptive optics-equipped ground based telescopes are obscured aperture systems, with a secondary mirror held in place by secondary support ‘spider’ vanes. The presence of a secondary obscuration can be dealt with by ingenious coronagraph designs, but the spider vanes themselves cause diffracted light that can hamper the search for jovian exoplanets around nearby stars. We look at the problem of suppressing spider vane diffraction in Lyot coronagraphs, including apodized pupil and band-limited designs. We show how spider vane diffraction can be reduced drastically, and in fact contained, in the final coronagraphic image, within one resolution element of the geometric image of the focal plane mask’s occulting spot. This makes adaptive optics coronagraphic searches for exojupiters possible on the next generation of adaptive optics systems being developed for 8–10 m class telescopes such as Gemini and the Very Large Telescopes.

Subject headings: instrumentation: adaptive optics — instrumentation: high angular resolution — space vehicles: instruments — techniques: high angular resolution — planetary systems

1. INTRODUCTION

In the last few years several exciting new coronagraphic designs have been proposed. These designs focus on suppressing starlight within a few resolution elements of bright stars in order to detect planetary companions of these stars fractions of an arcsecond from the star, a task which requires a contrast ratio of more than a million to one for extrasolar jovian planets (Burrows et al. 2004; Burrows 2005). An even more ambitious goal, that of detecting and characterizing extra-solar terrestrial planets, demands contrast ratios of a billion to one or higher.

Recent progress in coronagraphic concepts has yielded several classes of coronagraphs that achieve the requisite suppression in the ideal case (*e.g.*, Kuchner & Traub 2002; Soummer et al. 2003a,b; Kasdin et al. 2003; Guyon 2003), which generally requires zero wavefront error, and unobscured apertures. The fully-optimized, diffraction-limited Lyot project coronagraph (Lyot 1939; Sivaramakrishnan et al. 2001; Oppenheimer et al. 2003, 2004; Digby et al. 2004; Makidon et al. 2005), which is deployed at the Air Force AEOS 3.6m telescope (Roberts & Neyman 2002) is the first coronagraph to operate in the regime of ‘extreme adaptive optics’ (ExAO) with Strehl ratios around 90% under the best seeing conditions in the *H*-band. This instrument,

and all future ground and space coronagraphs, will have to work with non-zero wavefront error, and on aperture geometries subject to real-world engineering constraints. In Lloyd & Sivaramakrishnan (2005) and Sivaramakrishnan et al. (2005) we analyzed the effects of wavefront errors on Lyot coronagraphs. In this paper, we focus on the effects of spider diffraction in a Lyot coronagraph.

Next generation AO systems, designed for Gemini and an ESO Very Large Telescope, are likely to be dedicated to coronagraphic imaging and spectroscopy in the search for exo-jupiters. It is therefore important to understand and quantify the effects spiders have on coronagraphic imaging as these systems are designed and constructed over the next five years. This is particularly relevant in light of recent work on high dynamic range coronagraphy on obscured apertures (Soummer 2005).

We focus on an analytical treatment of this problem with the goal of producing some general understanding of the problem, not just a calculation for a specific case at a specific telescope. Over and above the narrow application of specific numerical calculations, there is a computational difficulty in modelling coronagraphs on obstructed apertures when taking spider vanes into account. For example, coronagraphic image simulations require about 6 to 8 samples across each resolution element in order to accurately model the effects of a $4\lambda/D$

¹ NSF Center for Adaptive Optics

image plane occulting stop (‘focal plane mask’) in the focal plane (λ being the central wavelength of the observing bandpass, and D the telescope diameter). This entails optical calculations using arrays 6 to 8 times the diameter of the entrance pupil. The 8 m Gemini telescope’s spider vanes are 1 cm thick. Thus the numerical arrays required to model the optical train can be 12000–16000 elements on a side. Furthermore, these numerical calculations can require extra-ordinary resolution and dynamic range to converge on the correct answer, and the effects of aliasing in an FFT can be quite severe at the 10^{-9} contrast level [*e.g.*, even very high resolution numerical calculations of the Four Quadrant Phase Mask coronagraph (Rouan et al. 2000) are inadequate to correctly calculate the coronagraphic point-spread function (PSF)], requiring an analytical solution (Lloyd et al. 2003). Fourier transform routines of optical modelling programs will need more memory than can be put in most of today’s computers. We are therefore forced to fall back on developing analytical estimates of the effect of secondary mirror support vanes on coronagraphic images. We treat classical Lyot coronagraphs (Lyot 1939) with their hard-edged, opaque focal plane masks; modified Lyot coronagraphs with graded focal plane masks described by Gaussian² or ‘band-limited’ (Kuchner & Traub 2002) functions; as well as apodized pupil Lyot coronagraphs (Soummer et al. 2003a; Soummer 2005). Guyon (2003) discusses pure pupil apodized high dynamic range imaging on arbitrarily-shaped apertures, Soummer et al. (2003b) treats dual-zone phase-mask coronagraphy on arbitrary apertures, and Lloyd et al. (2003) presents ways of dealing with four-quadrant phase mask coronagraphy on centrally-observed apertures with spiders.

2. MONOCHROMATIC CORONAGRAPHIC THEORY WITH SPIDER SUPPORTS

Here we briefly recapitulate our basic monochromatic Fourier optics formalism. A more detailed treatment can be found in Sivaramakrishnan et al. (2001); Lloyd & Sivaramakrishnan (2005). We recollect that a plane monochromatic wave travelling in the z direction in a homogenous medium without loss of energy can be characterized by a complex amplitude E representing the transverse (*e.g.*, electric) field strength of the wave. The full spatio-temporal expression for the field strength is $Ee^{i(\kappa z - \omega t)}$, where $\omega/\kappa = c$, the speed of the wave. We do not use the term *field* to denote image planes — the traditional optics usage — we always use the term to denote electromagnetic fields or scalar simplifications of them. The wavelength of the wave is $\lambda = 2\pi/\kappa$. The time-averaged intensity of a wave at a point is proportional to EE^* , where the average is taken over one period, $T = 2\pi/\omega$, of the harmonic wave. The phase of the complex number E represents a phase difference from the reference phase associated with the wave. A real, positive E corresponds to an electric field oscillating in phase with our reference wave. A purely imaginary positive value of E indicates that the electric field lags by a quarter cycle from the reference travelling wave. Transmission through passive, linear filters such as apertures, apodizers, and so forth, is represented by multiplying the field strength by the transmission of these objects which modify the wave.

² Ftacilas, private communication

Again, such multiplicative modification is accomplished using complex numbers to represent phase changes forced on the wave incident on such objects.

We assume that Fourier optics describes our imaging system: image field strengths are given by the Fourier transform of aperture (or pupil — we use the two terms interchangeably) illumination functions, and vice versa.

A telescope aperture is described by a transmission function pattern $A(x)$, where $x = (x_1, x_2)$ is the location in the aperture, in units of the wavelength of the light (see Fig. 1). The corresponding aperture illumination describing the electric field strength in the pupil (in response to an unaberrated, unit field strength, monochromatic incident wave) is $E_A = A(x)$. From this point onwards we drop the common factor $Ee^{i(\kappa z - \omega t)}$ when describing fields. The aperture intensities ($E_A E_A^*$) for two coronagraphic designs are shown in Fig. 2 (top row). The field strength in the image plane, $E_B = a(k)$, is the Fourier transform of E_A , where $k = (k_1, k_2)$ is the image plane coordinate in radians. Because of the Fourier relationship between pupil and image fields, k is also a spatial frequency vector for a given wavelength of light. We refer to this complex-valued field a as the ‘amplitude-spread function’ (ASF), by analogy with the PSF of an optical system. The PSF is aa^* . Our convention is to change the case of a function to indicate its Fourier transform. We multiply the image field E_B by a mask function $m(k)$ to model the focal plane mask of a coronagraph. The image field immediately after this mask is $E_C = m(k)E_B$. The electric field in the re-imaged pupil after the focal plane mask (the Lyot pupil, see Fig. 2, middle rows) is E_D , which is the Fourier transform of E_C . We use the fact that the transform of the image plane field E_B is just the aperture illumination function E_A itself, so the Lyot pupil field is $E_D = M(x)*E_A$, where $*$ is the convolution operator.

If the Lyot pupil stop transmission is $N(x)$, the electric field after the Lyot stop is $E_E = N(x)E_D$. The transform of this last expression is the final coronagraphic image field strength: $E_F = n(k)*[m(k)E_B]$. In this paper we look at the effects of secondary support spiders on the final coronagraphic PSF corresponding to the field strength E_F . We take into account the fact that $A(x)$ may be apodized (Fig. 2, right), so A is a graded function rather than a function that takes values of either 0 or 1. Understanding high dynamic range Lyot coronagraphy hinges on understanding the structure of the field strength E_D in the Lyot plane located at D, as well as the repercussions of such structure in the final image plane E_F .

3. SPIDER DIFFRACTION IN A LYOT CORONAGRAPH

The mask function in a Lyot coronagraph is best expressed as $m(k) = 1 - w(k)$, where $w(k)$ is the ‘focal plane mask shape’ function. For a hard-edged mask $w(k) = \Pi(D|k|/s)$, where s is the mask diameter in units of the resolution of the optical system, λ/D . The function $\Pi(\alpha)$ takes the value unity for $|\alpha| < 0.5$, and is zero elsewhere. We note that $w(0,0) = 1$ (which constrains $W(x)$ to have unit area). The Fourier transform of the focal plane mask transmission function $m(k)$ is $M(x) = \delta(x) - W(x)$, so the Lyot pupil electric field of a Lyot coronagraph can be expressed as

$$E_D = [\delta(x) - W(x)]*A(x). \quad (1)$$

(An example of the mask transmission function for a simple band-limited coronagraph is shown in Fig. 3.)

We must understand the morphology of the Lyot pupil field in order to understand the extent to which secondary spider supports reduce the final coronagraphic image's dynamic range.

We model a single spider vane across the entrance pupil of a telescope by writing

$$E_A = A(x)(1 - \Pi(x_1/\epsilon)) \quad (2)$$

(ϵ being the width of the spider vane). Secondary obstructions result in different effects. We do not treat them here (see *e.g.*, Sivaramakrishnan et al. 2001; Lloyd et al. 2003, for details on this topic). Equation (1) with this aperture function produces a Lyot pupil field

$$E_L = A(x)(1 - \Pi(x_1/\epsilon)*\delta(x_2)) - W(x)*[A(x)(1 - \Pi(x_1/\epsilon)*\delta(x_2))]. \quad (3)$$

We are only concerned with the ‘interior’ of the aperture in the Lyot plane, where, by design, we are satisfied with coronagraphic performance of our aperture without spider support vanes. This means that in our estimation, $A(x) - W*A(x)$ is sufficiently small for our scientific purposes (*e.g.*, Soummer et al. 2003a; Soummer 2005) or zero (Rouan et al. 2000; Aime et al. 2001, 2002; Kuchner & Traub 2002; Soummer et al. 2003b). We therefore drop this component of equation (3), so in the interior of the Lyot pupil we obtain

$$E_{L, \text{interior}} = A(x)[\Pi(x_1/\epsilon)*\delta(x_2)] - W(x)*(A(x)\Pi(x_1/\epsilon)*\delta(x_2)). \quad (4)$$

This is the contribution (in the Lyot pupil) due to diffraction from a long thin obstruction such as a spider vane in the entrance aperture.

Fig. 2 (left) shows the intensity of the Lyot pupil field using a perfect theoretical coronagraph, the band-limited coronagraph, where, in the absence of spider vanes and optical aberrations, the interior of the Lyot field is identically zero.

There are two components to the field strength in the interior region of the Lyot pupil. The bright central stripe is exactly the spider vane width ϵ — its brightness is very close to that of the brightness of the clear or apodized aperture in the entrance pupil. This is the first term in equation (4), *viz.*, $A(x)[\Pi(x/\epsilon)*\delta(x_2)]$. For high dynamic range applications it can be masked out with a thin opaque strip in the Lyot pupil stop. This strip can be oversized for practical reasons without noticeably affecting throughput at the Lyot stop. We call this kind of Lyot stop a ‘Lyot spider stop’. It resembles the ‘reticulated Lyot stop’ of Sivaramakrishnan & Yaitskova (2005), which masks out bright inter-segment gaps in the coronagraphic Lyot plane of extremely large, highly-segmented telescopes.

The extended low-intensity ‘aura’ of the bright spider vane is described by the second term in equation (4), $-W(x)*(A(x)\Pi(x_1/\epsilon)*\delta(x_2))$ (Fig. 2, bottom row). For the applications we consider here, the equivalent width of the function $W(x)$ is of order D/s , since we wish to search for faint companions and structure outside an inner working angle of about $s\lambda/2D$ of a bright, on-axis star. Typically s will lie between 4 and 10.

When the width of the focal plane mask becomes larger than $\sim 10\lambda/D$, this strip of dimmer light can be removed by a Lyot pupil stop with an oversized spider vane

obstruction without sacrificing Lyot stop throughput too much. We point out that the exact geometry of the spiders is not relevant — our approach can deal with non-orthogonal spiders as easily as with perfectly aligned spiders.

3.1. The coronagraphic PSF with spiders

We now estimate the field strength in the final coronagraphic image with a Lyot spider stop. The coronagraphic ASF without a Lyot stop of any kind is the Fourier transform of the field in the interior of the Lyot pupil described by equation (4):

$$a_c(k) = \epsilon a(k)*\text{sinc}(\epsilon k_1) - \epsilon w(k)(a(k)*\text{sinc}(\epsilon k_1)). \quad (5)$$

The first term of the ASF $a_c(k)$ is $\epsilon a(k)*[\text{sinc}(\epsilon k_1)]$. This has the shape of a regular spider diffraction spike, but is down a factor ϵ^2 in intensity from the direct image's spider spike. Masking out the bright spider vane removes this first term in the expression for $a_c(k)$. The remaining term is modulated by the mask shape function $m(k)$ itself. If the mask shape is the circular top hat function $\Pi(D|k|/s)$, spider diffraction in the coronagraphic image plane is confined to the region behind the mask when a Lyot spider stop is used. The $\text{sinc}(\epsilon k_1)$ function describes the direct image's spider profile along the length of the spider ‘spike’ in the image plane. This function is close to unity in the region behind or just around the focal plane mask in the direct or coronagraphic image planes. $w(k)$ is also unity at scales where $a(k)$ is significant in size if the focal plane mask is a few to several resolution elements wide. Thus, where $w(k)$ is non-zero (for hard-edged masks), $a(k)*\text{sinc}(\epsilon k_1)$ is very close to the integral of $a(k)$ over its entire domain. The value of this integral is $A(0)$ because of the Fourier relation between a and A . We stress that we are trying to estimate the size of the spider effects here rather than calculate them exactly.

However, we should consider an appropriately optimized Lyot stop — on a traditional or ‘classical’ Lyot coronagraph (or a band-limited coronagraph) this stop is undersized relative to the entrance pupil. In apodized pupil Lyot coronagraphs, the Lyot stop is not undersized; it lets the entire graded entrance pupil through. In the former case we would need to convolve $a_c(k)$ by the Fourier transform of this undersized pupil. If the undersized classical Lyot stop is described by the function $A'(x)$, the classical or band-limited coronagraph's ASF is

$$a_{c,LC}(k) = \epsilon a'(k)*\text{sinc}(\epsilon k_1) - \epsilon a'(k)*[w(k)(a(k)*\text{sinc}(\epsilon k_1))] \quad (6)$$

(we note that $a'(k)*a(k) = a'(k)$ if the Lyot stop and entrance pupil are not apodized, and the Lyot stop support is a subset of the entrance pupil support).

With a Lyot spider stop the first term disappears, leaving only the second term in equation (6). We see from this that the effects of spider diffraction are now concentrated behind the mask, as in the case of a_c , but because of a convolution with $a'(k)$, the diffracted light leaks out about a diffraction width outside the actual mask (in the final coronagraphic image plane). Thus we can immediately conclude that for a hard-edged focal plane mask with diameter $s\lambda/D$, combined with an optimized Lyot

spider stop, residual spider diffraction is very small outside a circle of diameter $s\lambda/D + \lambda/D'$ around the on-axis star (D' being the Lyot stop outer diameter, projected back to the primary mirror). Extending this argument to obstructed apertures is straightforward: the spider diffraction will fall drastically at about a PSF equivalent width away from the geometric shadow of the focal plane mask in the final image plane. The secondary obstruction will make for a larger distance scale for the fall-off of residual spider diffraction outside the focal plane mask's edge. For graded focal plane masks (such as Gaussian or band-limited coronagraphs), residual spider diffraction after using an optimized Lyot spider stop extends everywhere that the mask shape function is non-zero.

Monochromatic coronagraphic images using a simple and a spider Lyot stop in a band-limited coronagraph are shown in Fig. 4, cases *BL-a* and *BL-b* respectively. Here the perfect coronagraph on a clear unobstructed aperture with no phase or amplitude errors produces no on-axis light whatsoever in the Lyot pupil after it is stopped down by the Lyot stop (Fig. 2, in the 'no spider' column's Lyot stop intensity), or in the following coronagraphic image plane. A Lyot stop optimized without consideration of spider vanes lets through a horizontally-oriented 'spider spike' of light (Fig. 4, *BL-a*). If there were two crossed spider vanes across the aperture, this image would show the usual cross observers associate with secondary support spiders. The 'ringing' in the vertical direction has a period of the resolution element induced by the Lyot stop: approximately twice the size of the non-coronagraphic resolution λ/D for this design. Removal of the bright strip of light from the Lyot plane (where the geometrical image of the spider vane is located) by using a Lyot spider stop removes much of the light from the coronagraphic image (Fig. 4, *BL-b*). The dark vertical stripes are located at multiples of $8\lambda/D$ in this panel. The focal plane mask structure of the band-limited coronagraph design in this example is seen by comparing this residual coronagraphic image with the focal plane mask itself (shown in Fig. 3).

For the apodized pupil Lyot coronagraph the convolution is with the Fourier transform of the full entrance pupil without apodization. This coronagraphic design does not undersize the Lyot pupil, so $D' = D$. For the unobscured aperture with a spider, this Fourier transform is the jinc function, $2J_1(x)/x$ (where $J_1(x)$ is the Bessel function of the first kind, with index 1) —

$$a_{c,APLC}(k) = \epsilon \text{jinc}(Dk) * a(k) * \text{sinc}(\epsilon k_1) - \epsilon \text{jinc}(Dk) * [w(k)(a(k) * \text{sinc}(\epsilon k_1))]. \quad (7)$$

We can treat centrally obscured apertures by using the difference of two jinc functions, although for simplicity we show the unobscured aperture case here. Once again, an optimized Lyot spider stop will remove the first term in equation (7), leaving the second term. This term is reduced in field strength by a factor ϵ from what is essentially $A(0, 0)$, and it is also restricted to a diffraction-width (or equivalent width of the PSF for obscured apertures) around the the projection of the focal plane mask on the final coronagraphic image plane.

3.2. Apodized pupil and apodized occulter coronagraphs

On a telescope with a secondary mirror obstructing the entrance aperture, it is possible to design Lyot coro-

graphs such as apodized pupil Lyots, and Gaussian or band-limited coronagraphs. The presence of spider vanes makes the apodized pupil design preferable to the apodized occulter designs. If we examine Figs. 2 and 4 in the case of the theoretically perfect band-limited design we can understand why this is the case.

The focal plane mask used in this example possesses a $1 - \text{jinc}(\alpha k)$ transmission function. α is chosen to produce a first zero in the jinc function at $k = 8\lambda/D$. The width of the residual broad swath of low intensity light is twice the bandwidth or equivalent width of the function describing the focal plane mask (Fig. 2, Lyot plane on the left).

In the image plane of the band-limited coronagraph with the Lyot spider stop (Fig. 4 *BL-b*), we see that light diffracted by the spider vane spills into the coronagraphic image plane wherever the focal plane mask has a transmission that is not unity, *i.e.*, wherever our focal plane mask had any opacity whatsoever. In fact the light occupies a slightly larger area (by about one resolution element) of the image after passage through an undersized Lyot stop.

With an apodized pupil design that utilizes a hard-edged focal plane mask, the on-axis coronagraphic image (which is due almost entirely to spider vane diffraction when we use our analytical, circularly-symmetric apodizer) is localized to a circular area with a radius one resolution element larger than the original focal plane mask (Fig. 4 *AP-b*). Thus, for the 8 m Gemini telescope with an apodized pupil Lyot coronagraph with a $4\lambda/D$ diameter focal plane mask, all diffraction from the spider vanes is restricted to a disk $6\lambda/D$ in diameter. Furthermore, the contrast ratio between this diffracted light and a PSF taken with the same apodizer and Lyot stop, but no focal plane stop, is of the order of 10^{-6} with a simple analytical apodizer design.

This is visible in Fig. 4, where we see the structure of the focal plane mask in residual spider diffraction after using a Lyot spider stop. We simulated a single spider vane three pixels wide across a 170 pixel diameter aperture. We calculated the PSFs with the band-limited design described here, as well as with a numerical approximation of an analytical apodized pupil Lyot coronagraph optimized for a circular pupil (Soummer et al. 2003a). While Soummer (2005) shows that it is possible to refine the apodized pupil coronagraph design to accommodate spiders, we used the circular aperture apodizer design because an azimuthally symmetric apodizer is easier to align in practice, and the analytical apodizing function is easy to generate numerically. The particular example we present is taken from Soummer et al. (2003a). It has a 19% throughput apodizer matched to a $3.74\lambda/D$ focal plane mask diameter. Figs. 5 and 6 show cuts through the PSFs of both designs, with and without Lyot spider stops. These cuts show that the apodized pupil coronagraphic design outperforms the band-limited design away from residual spider spikes in the coronagraphic image when the bright spiders are blocked in the Lyot pupil, in spite of the fact that the apodized pupil design's focal plane mask equivalent width is smaller than that of our band-limited example. This localization of diffracted light due to spiders suggests that apodized pupil coronagraphic designs suit future ground-based adaptive optics coronagraphic instruments on existing telescopes.

4. DISCUSSION

We have demonstrated that even after masking out bright spiders in the Lyot plane of a Lyot coronagraph, some residual spider diffraction will be seen around the focal plane mask in the coronagraphic image. These effects cause a brightness proportional to the square of the spider thickness, but are localized to a PSF-width around the focal plane mask. Hard-edged masks show a stronger localization of the light diffracted by spiders than Gaussian or band-limited masks. This localization is desirable behavior for an extreme adaptive optics coronagraph on existing 8–10 m class telescopes, all of which possess secondary mirror support spider vanes.

The residual brightness due to spider vane diffraction will affect speckle statistics in this region (Aime & Soummer 2004), inducing a larger variance in intensity there. However, on hard-edged focal plane mask coronagraphs, masking out the bright spiders in the Lyot plane does enable good suppression of spider diffraction just one resolution element away from the mask edge. Opto-mechanical tolerances for on-axis telescope designs are looser than for extreme off-axis designs. The advent of on-axis apodized pupil Lyot coronagraphs with good suppression of on-axis sources (Soummer 2005) makes it important to understand the effects of spiders in Lyot coronagraphs and their modern variants when

designing coronagraphs to search for extrasolar jovian companions using ground-based, next-generation adaptive optics systems on today's 8–10 m class telescopes.

We acknowledge frequent helpful discussions with R. Soummer, and his generous contribution of a numerical realization of the apodized pupil Lyot coronagraph on an unobstructed circular aperture. We are grateful to the referee for useful comments, and to P. E. Hodge, P. Greenfield, J. T. Miller, and N. Dencheva for their role in developing and supporting the Python Numarray module (Greenfield et al. 2002; Greenfield et al. 2003), wrapping the numerical Fourier transform library FFTW (Frigo & Johnson 1997) for Numarray, and providing support for matplotlib (Hunter 2005). We also thank the Space Telescope Science Institute's Research Programs Office and Director's Discretionary Research Fund for support. This work has also been supported by the National Science Foundation Science and Technology Center for Adaptive Optics, managed by the University of California at Santa Cruz under cooperative agreement No. AST-9876783, and by the National Science Foundation under Grant No. AST-0215793 and Grant No. AST-0334916.

REFERENCES

- Aime, C. & Soummer, R. 2004, *ApJ*, 612, L85
Aime, C., Soummer, R., & Ferrari, A. 2001, *A&A*, 379, 697
—, 2002, *A&A*, 389, 334
Burrows, A. 2005, *Nature*, 433, 261
Burrows, A., Sudarsky, D., & Hubeny, I. 2004, *ApJ*, 609, 407
Digby, A. P., Oppenheimer, B. R., Newburgh, L., Brenner, D., Shara, M., Mey, J., Mandeville, C., Makidon, R. B., Sivaramakrishnan, A., Soummer, R., Graham, J. R., Kalas, P., Perrin, M. D., Roberts, L. C., Kuhn, J., Whitman, K., & Lloyd, J. P. 2004, in *Proc. SPIE Vol. 5490, Advances in Adaptive Optics*, Roberto Ragazzoni and Domenico Bonaccini; Eds.
Frigo, M. & Johnson, S. G. 1997, in *Technical Report MIT-LCS-TR-728* (Massachusetts Institute of Technology)
Greenfield, P., Miller, J. T., Hsu, J.-C., & White, R. L. 2003, in *PyCon 2003 Proceedings*, ed. S. Holden
Greenfield, P., Miller, T., Hsu, J.-C., & White, R. L. 2002, in *ASP Conf. Ser. 281: Astronomical Data Analysis Software and Systems XI*, 140–+
Guyon, O. 2003, *A&A*, 404, 379
Hunter, J. 2005, *The Matplotlib User's Guide* (University of Chicago Medical School)
Kasdin, N. J., Vanderbei, R. J., Spergel, D. N., & Littman, M. G. 2003, *ApJ*, 582, 1147
Kuchner, M. J. & Traub, W. A. 2002, *ApJ*, 570, 900
Lloyd, J. P., Gavel, D. T., Graham, J. R., Hodge, P. E., Sivaramakrishnan, A., & Voit, G. M. 2003, in *High-Contrast Imaging for Exo-Planet Detection*. Edited by Alfred B. Schultz. *Proceedings of the SPIE*, Volume 4860, pp. 171-181 (2003), 171–181
Lloyd, J. P. & Sivaramakrishnan, A. 2005, *ApJ*, 621, 1153
Lyot, B. 1939, *MNRAS*, 99, 580
Makidon, R. B., Sivaramakrishnan, A., Perrin, M. D., i Roberts, L. C., Oppenheimer, B. R., Soummer, R., & Graham, J. R. 2005, *PASP*, in press
Oppenheimer, B. R., Digby, A. P., Newburgh, L., Brenner, D., Shara, M., Mey, J., Mandeville, C., Makidon, R. B., Sivaramakrishnan, A., Soummer, R., Graham, J. R., Kalas, P., Perrin, M. D., Roberts, L. C., Kuhn, J., Whitman, K., & Lloyd, J. P. 2004, in *Proc. SPIE Vol. 5490, Advances in Adaptive Optics*, Roberto Ragazzoni and Domenico Bonaccini; Eds.
Oppenheimer, B. R., Sivaramakrishnan, A., & Makidon, R. B. 2003, *Imaging Exoplanets: The Role of Small Telescopes (The Future of Small Telescopes In The New Millennium. Volume III - Science in the Shadow of Giants)*, 155
Roberts, L. C. & Neyman, C. R. 2002, *PASP*, 114, 1260
Rouan, D., Riaud, P., Boccaletti, A., Clénet, Y., & Labeyrie, A. 2000, *PASP*, 112, 1479
Sivaramakrishnan, A., Koresko, C. D., Makidon, R. B., Berkefeld, T., & Kuchner, M. J. 2001, *ApJ*, 552, 397
Sivaramakrishnan, A., Soummer, R., Sivaramakrishnan, A. V., Lloyd, J. P., Oppenheimer, B. R., Perrin, M. D., & Makidon, R. B. 2005, *ApJ*, submitted
Sivaramakrishnan, A. & Yaitskova, N. 2005, *ApJ*, 626, L65
Soummer, R. 2005, *ApJ*, 618, L161
Soummer, R., Aime, C., & Falloon, P. E. 2003a, *A&A*, 397, 1161
Soummer, R., Dohlen, K., & Aime, C. 2003b, *A&A*, 403, 369

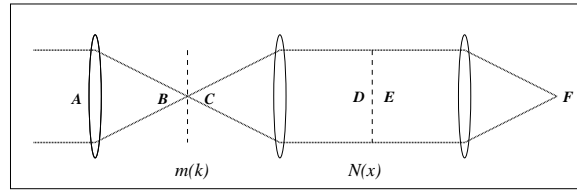


FIG. 1.— The essential planes and stops in a coronagraph. The entrance aperture is A, the direct image at B falls on a focal plane mask whose transmission function is $m(k)$. The re-imaged pupil plane D, after being modified by passage through a Lyot stop with a transmission function $N(x)$, is sent to the coronagraphic image at F.

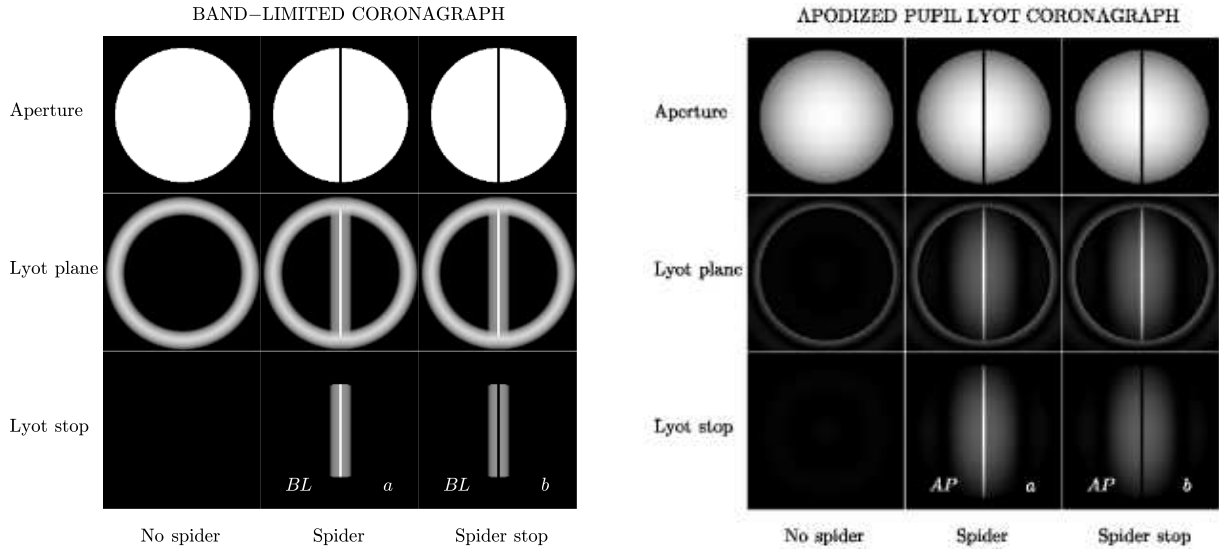


FIG. 2.— Key planes of a monochromatic, band-limited coronagraph and an apodized pupil Lyot coronagraph on a circular, unaberrated aperture with and without a single spider vane. Intensity in the various pupil planes are shown on the same logarithmic greyscale between 1 and 1.0×10^{-4} . The perfect coronagraph on a clear aperture with no spider vane obstruction (“No spider” columns) produces a sufficiently dark Lyot pupil interior, as is seen in the “Lyot plane” rows. The “Lyot stop” rows show two styles of Lyot stops used. Left and middle, a simple Lyot stop removes all incoming on-axis light on the external edge of the entrance pupil. In the presence of a spider vane the simple Lyot stop leaves the bright strip of light in the geometrical image of the spider vane, and the ‘aura’ of surrounding light, whose intensity is proportional to the square of the ratio of the spider vane thickness to the telescope diameter. At right, a Lyot stop which removes the bright strip of light located at the spider vane position itself.

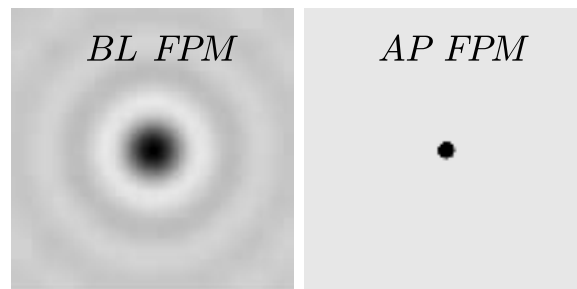


FIG. 3.— The transmission of the focal plane masks of the band-limited (BL) and apodized pupil (AP) Lyot coronagraph designs shown in Fig. 2. The first zero of the BL mask transmission profile (a $1 - \text{jinc}$ function) occurs at $8\lambda/D$. The images shown are $64\lambda/D$ across. This band-limited function is unphysical in that the transmission of the mask exceeds unity in some regions, although this detail does not complicate our analysis nor invalidate our conclusions. This mask induces a scale of $D/8$ in the Lyot pupil plane, which is seen in the residual spider diffraction shown in the panel (BL b) of Fig. 4. The AP mask is $3.74\lambda/D$ across.

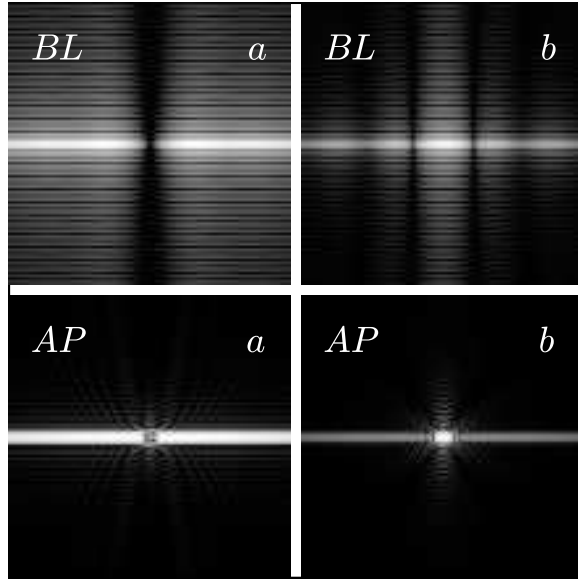


FIG. 4.— Coronagraphic on-axis PSF of an apodized pupil (AP) and band-limited (BL) Lyot coronagraph in the presence of a single spider vane. Without blocking the bright spider vanes in the Lyot pupil [case (a)], the band-limited coronagraph shows better suppression of light from an on-axis star than the apodized pupil Lyot coronagraph. When bright spider vanes in the Lyot plane are blocked [case (b)], the apodized pupil Lyot coronagraph performs better than the band-limited design. The apodized design focal plane mask diameter is $3.74\lambda/D$, and the band-limited mask is the same as that described in 3, with a scale size of $8\lambda/D$. A logarithmic stretch between 1.0×10^{-3} and 1.0×10^{-8} is used for all these images. Normalization is such that the peak intensity of the PSF without a focal plane mask, but through the optimized Lyot stop without spider obstructions is unity.

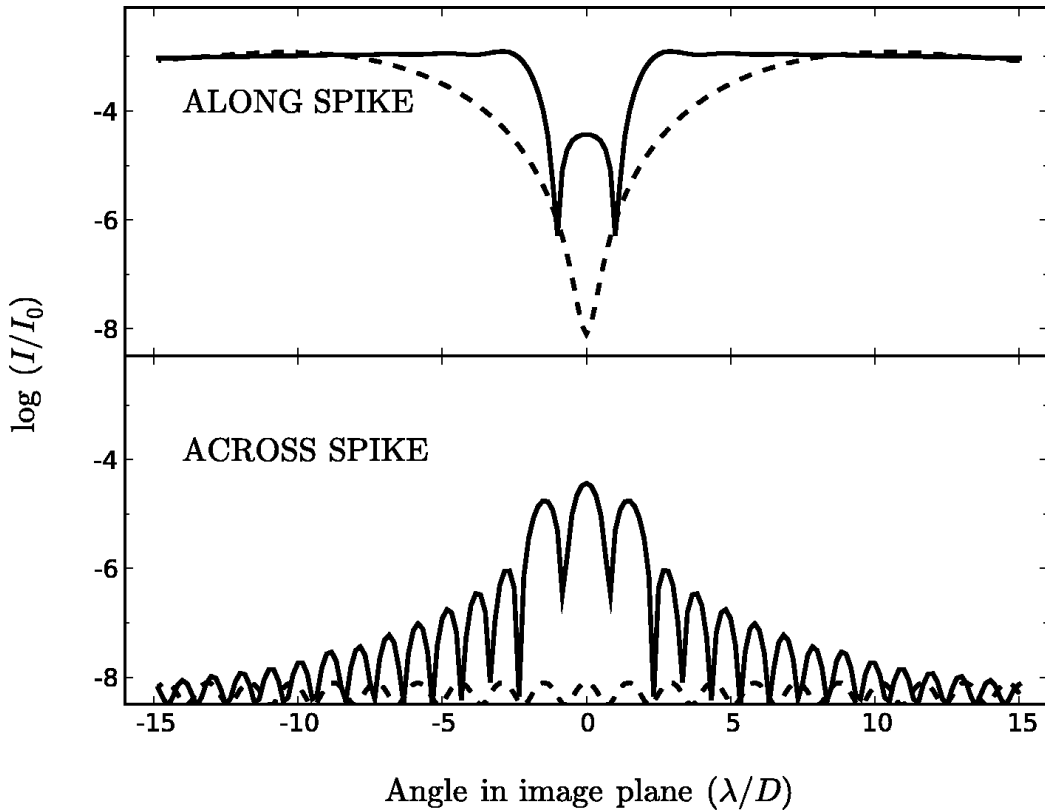


FIG. 5.— Logarithmic intensity profiles of the coronagraphic PSF of the designs shown in Fig. 4. Here the optimized Lyot stop does not block out the single spider vane. Diffracted light from the spider reduces contrast significantly. We utilize the same PSF normalization as in Fig. 4. The solid curve shows the apodized pupil Lyot coronagraphic PSF profile and the dashed line shows the band-limited coronagraphic PSF profile (panel *AP-a* and *BL-a* in Fig. 4). In this case coronagraphic performance is poor, although the band-limited design is less susceptible to diffracted light from the spider vane.

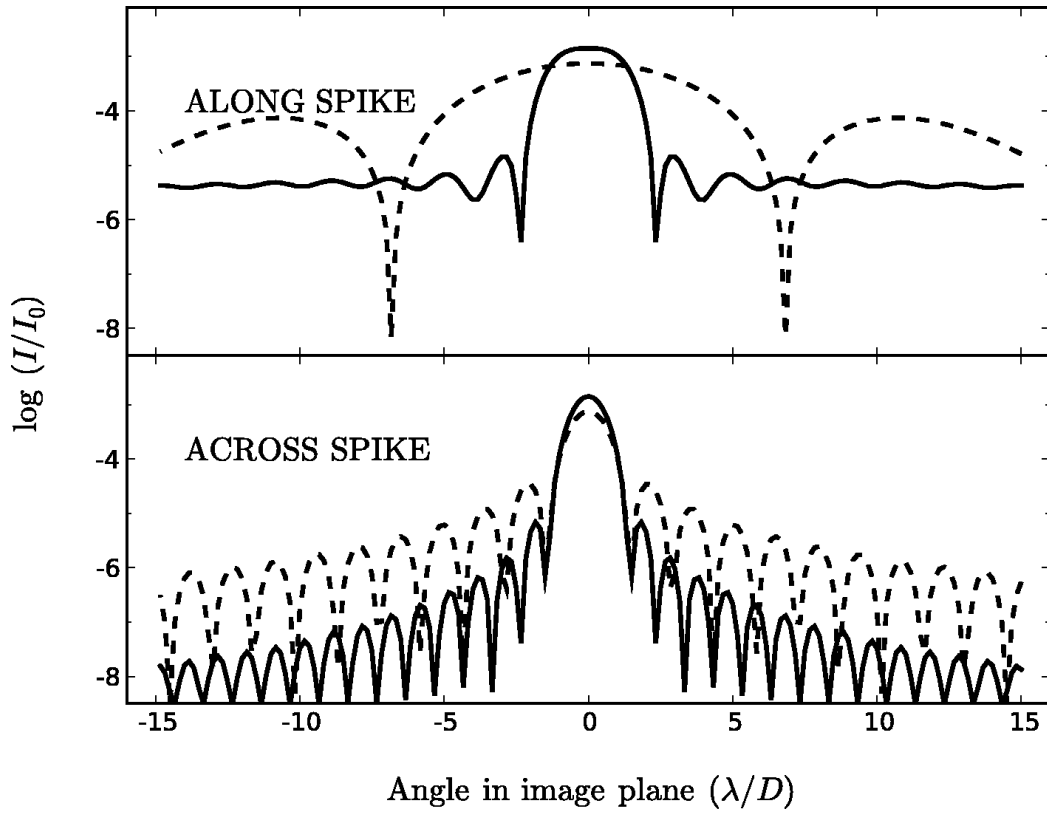


FIG. 6.— Logarithmic intensity profiles of the coronagraphic PSF of the same designs shown in Fig. 4. In contrast with Fig. 5, here the optimized Lyot stop blocks out the single spider vane. Diffracted light from the spider is thereby suppressed greatly. We utilize the same PSF normalization as in Fig. 4. The solid curve shows the apodized pupil Lyot coronagraphic PSF profile, and the dashed line shows the band-limited coronagraphic PSF profile (panel *AP-b* and *BL-b* in Fig. 4). In this case coronagraphic performance is much improved, and the apodized pupil design contains the spread of the residual light diffracted by the spider far better than does the band-limited design. The PSF of the apodized pupil Lyot coronagraph drops quickly with distance from the residual bright spider spike seen in panel *AP-b* of Fig. 4.